NANO LETTERS

pubs.acs.org/NanoLett Letter

Ultra-photostable DNA FluoroCubes: Mechanism of Photostability and Compatibility with FRET and Dark Quenching

Aaron T. Blanchard, Zi Li, Elizabeth C. Duran, Catherine E. Scull, J. Damon Hoff, Keenan R. Wright, Victor Pan, and Nils G. Walter*

Cite This: *Nano Lett.* 2022, 22, 6235−6244 Read Online

ACCESS | Metrics & More | Article Recommendations | Supporting Information

ABSTRACT: DNA-based FluoroCubes were recently developed as a solution to photobleaching, which is a ubiquitous limitation of fluorescence microscopy (Niekamp; Stuurman; Vale *Nature Methods*, **2020**). FluoroCubes, which are not as compact ∼4 × 4 × 5.4 nm^3 four-helix bundles coupled to ≤6 fluorescent dyes, remain fluorescent up to ∼50× longer than single dyes and emit up to ∼40× as many photons. The current work answers two important questions about FluoroCubes. First, what is the mechanism by which photostability is enhanced? Second, are FluoroCubes compatible with Förster resonance energy transfer (FRET) and similar techniques? We use single particle photobleaching studies to show that photostability arises through interactions between the fluorophores and the four-helix DNA bundle. Supporting this, we discover that smaller ∼4 × 4 × 2.7 nm^3 FluoroCubes also confer ultraphotostability. However, we find that certain dye−dye interactions negatively impact FluoroCube performance. Accordingly, 4-dye FluoroCubes lacking these interactions perform better than 6-dye FluoroCubes. We also demonstrate that FluoroCubes are compatible with FRET and dark quenching applications.

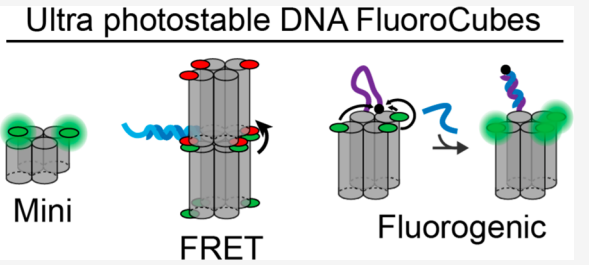

KEYWORDS: *DNA nanotechnology, fluorescence microscopy, single molecule imaging, FRET, fluorogenic probes*

Photobleaching, a process wherein fluorescent dyes irreversibly degrade due to excitation, is a nearly ubiquitous limitation in fluorescence microscopy. Photobleaching limits observation time in temporal studies, limits spatial resolution in single molecule imaging, and biases data from fluorescent sensors designed to undergo brightness changes for biological research. A variety of solutions to this challenge have been presented, including the synthesis of photostable dyes,[1−3] the use of oxygen scavenging system (OSS)s and triplet state quenchers,[4−6] encapsulation of fluorophores within protective nanostructures,[7−11] and the creation of fluorescent nanoparticles such as quantum dots.[12] A promising recent development was the invention of ultra-photostable DNA-based FluoroCubes.[13] DNA FluoroCubes consist of four 32-nucleotide (nt) DNA strands that, when annealed together, assemble into a compact four-helix bundle with approximate dimensions of 4.0 × 4.0 × 5.6 nm^3 (Scheme 1a, Figure 1a). Three of the strands (called the A-, B-, and C-strands) are covalently labeled with fluorescent dyes at both termini, while the fourth strand (the ligand strand) presents a ligand, such as biotin, that can link the FluoroCube to a molecule of interest such as streptavidin (SA).

These compact 6-dye nanostructures are much less sensitive to photobleaching than single dyes.[13] Most notably, FluoroCubes carrying the widely used Cyanine 3 (Cy3) fluorophore were reported to exhibit a 54× increase (relative to a single Cy3 on a DNA duplex) in half-life (τ) and a 43× increase in the total photon count before photobleaching ($N_{photons}$).[13] FluoroCube-based photostability enhancement is additive with enhancements offered by both OSSs[4,5] and dye modifications (e.g., the engineered Cy3N and ATTO 647N dyes). Combining these approaches provides total photostability that is unparalleled among organic dyes and rivals that of quantum dot nanocrystals.[13] Many questions remain unanswered about the physical underpinnings of this photostability.

FluoroCubes have enabled high precision particle tracking experiments for the long-term study of molecular motors,[13,14] and there are many additional potential application areas for FluoroCube technology. One useful feature in fluorescence is the ability to directly interrogate molecular interactions and conformations using Förster resonance energy transfer (FRET).[15−17] FRET is a process wherein energy transfers from an excited donor fluorophore to an acceptor fluorophore within a characteristic radius of typically ∼5 nm. The

Received: May 4, 2022
Revised: June 30, 2022
Published: July 26, 2022

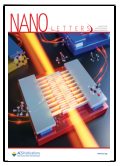

https://doi.org/10.1021/acs.nanolett.2c01757
Nano Lett. 2022, 22, 6235−6244

Scheme 1. FluoroCube assembly and constructs[a]

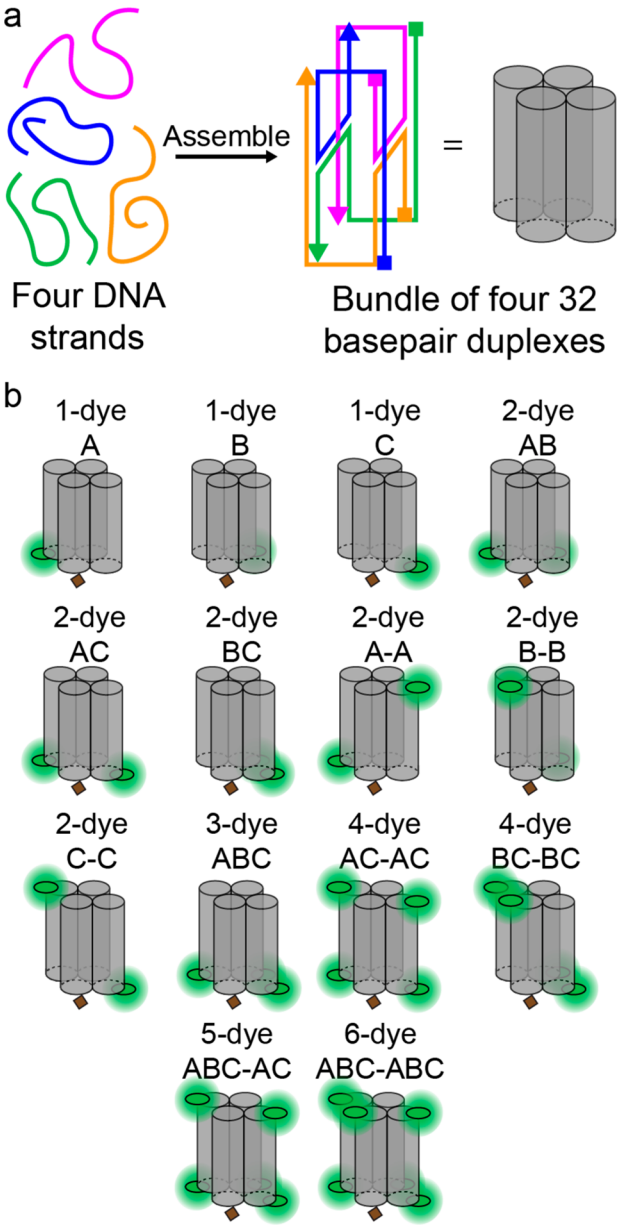

[a](a) Assembly of a DNA FluoroCube nanostructure from four 32 nucleotide DNA strands. (b) The 14 constructs studied in this work, each with Cy3 dyes strategically conjugated to different combinations of DNA strand termini.

transferred energy is then emitted by the acceptor, resulting in emission that is red-shifted relative to the emission of the donor. FRET is used in a wide range of applications, including single molecule biophysics,[15] cellular biology,[17,18] and molecular sensing.[16,19]

A similar class of techniques utilizes dark acceptors (also called quenchers), which accept energy transfer but do not emit fluorescence. Dark quenchers are useful for conditional quenching applications, wherein donor-quencher separation produces a very large increase in fluorescence intensity for reporting on conformational changes such as DNA or RNA hybridization[20−23] or molecular tension.[24,25] In some cases, very close contact between dark quenchers and donor fluorophores can result in ground state stabilization (or "contact quenching"), wherein electronic coupling prevents donor excitation altogether.[26] We here aimed to test whether FluoroCubes are compatible with FRET and conditional quenching. To understand compatibility between these techniques and FluoroCubes, we first studied the mechanism through which FluoroCubes confer ultraphotostability.

Simple linear scaling of fluorescence with the number of dyes (n) would predict $N_{photons} \propto n$ and $\tau \propto \log(n + 1)$ (approximately, see Supporting Information Note 1). However, $\log(7) \approx 2$, which is smaller by an order of magnitude than the observed increase in τ (10−54× reported, depending on the dye[13]). Dye−dye and/or dye−DNA nanostructure interactions thus appear to enhance photostability. Interactions between dyes like Cy3 and DNA nanostructures have been shown to enhance photostability in certain contexts.[27,28] Dye−dye interactions, such as the formation of electronically coupled dye-aggregates[29−32] can also contribute to photostabilization in some cases.[33] Previous experiments[13] showed that preventing dye−dye interactions by spacing Cy3 dyes out on a larger DNA origami cube (~8 × 8 × 11 nm^3) resulted in $N_{photons}$ and τ-values that are vastly improved relative to single dsDNA-conjugated dyes, but still about 2× lower than Cy3 FluoroCubes. This led us (and others)[34] to hypothesize that both dye−dye interactions and dye−DNA interactions (i.e., interactions between individual dyes and the surface of the DNA 4-helix bundle), contribute to increased photostability.

To test this proposed model, we assembled 14 FluoroCube constructs with $1 \leq n \leq 6$ and different fluorophore positions (Scheme 1b, Figure S1, Tables S1−2). Specifically, we assembled three 1-dye constructs (1-dye A, 1-dye B, and 1-dye C, where the letter denotes whether the dye is conjugated to the A-strand, B-strand, or C-strand), three 2-dye constructs with fluorophores on the same side of the FluoroCube (2-dye AB, 2-dye AC, and 2-dye BC), three 2-dye constructs with fluorophores on opposite sides of the FluoroCube (2-dye A-A, 2-dye B-B, and 2-dye C-C), a 3-dye construct with fluorophores all on one side of the FluoroCube (3-dye ABC), two 4-dye constructs with two fluorophores on each side (4-dye AC-AC, and 4-dye BC-BC), and 5- and 6-dye constructs (5-dye ABC-AC and 6-dye ABC-ABC).

We immobilized these constructs onto glass coverslips at low surface densities via biotin−streptavidin binding (Figure 1b). We then performed single molecule photobleaching studies of these FluoroCubes (Figures 1d,e, S2) by imaging continuously for ≥10 min using total internal reflection fluorescence (TIRF) microscopy in the presence of an OSS containing PCA/PCD and the triplet state quencher Trolox.[4,5] As previously observed,[13] FluoroCubes exhibited large fluctuations in fluorescence intensity (Figure 1f). We also tested 1- and 2-dye FluoroCubes assembled from two oligonucleotides only, which are expected to be 50% smaller by volume than 4-strand FluoroCubes (4 × 4 × 2.7 nm^3, Figures 1c, S3). For all constructs, the average FluoroCube fluorescence intensity, $\langle I \rangle$, accurately fit a single-exponential decay model (Figures 1g and S4)

$$\langle I \rangle = I_0 \exp(-k_1 t) \quad (1)$$

where the initial intensity, I_0, and the single-dye bleach rate, k_1, are fit parameters, and t denotes the duration of laser illumination and imaging. Because n photobleaching steps must occur prior to total photobleaching, the fraction (f) of remaining bright FluoroCubes (assuming equal bleaching rates of all n dyes) can be described by

https://doi.org/10.1021/acs.nanolett.2c01757
Nano Lett. 2022, 22, 6235−6244

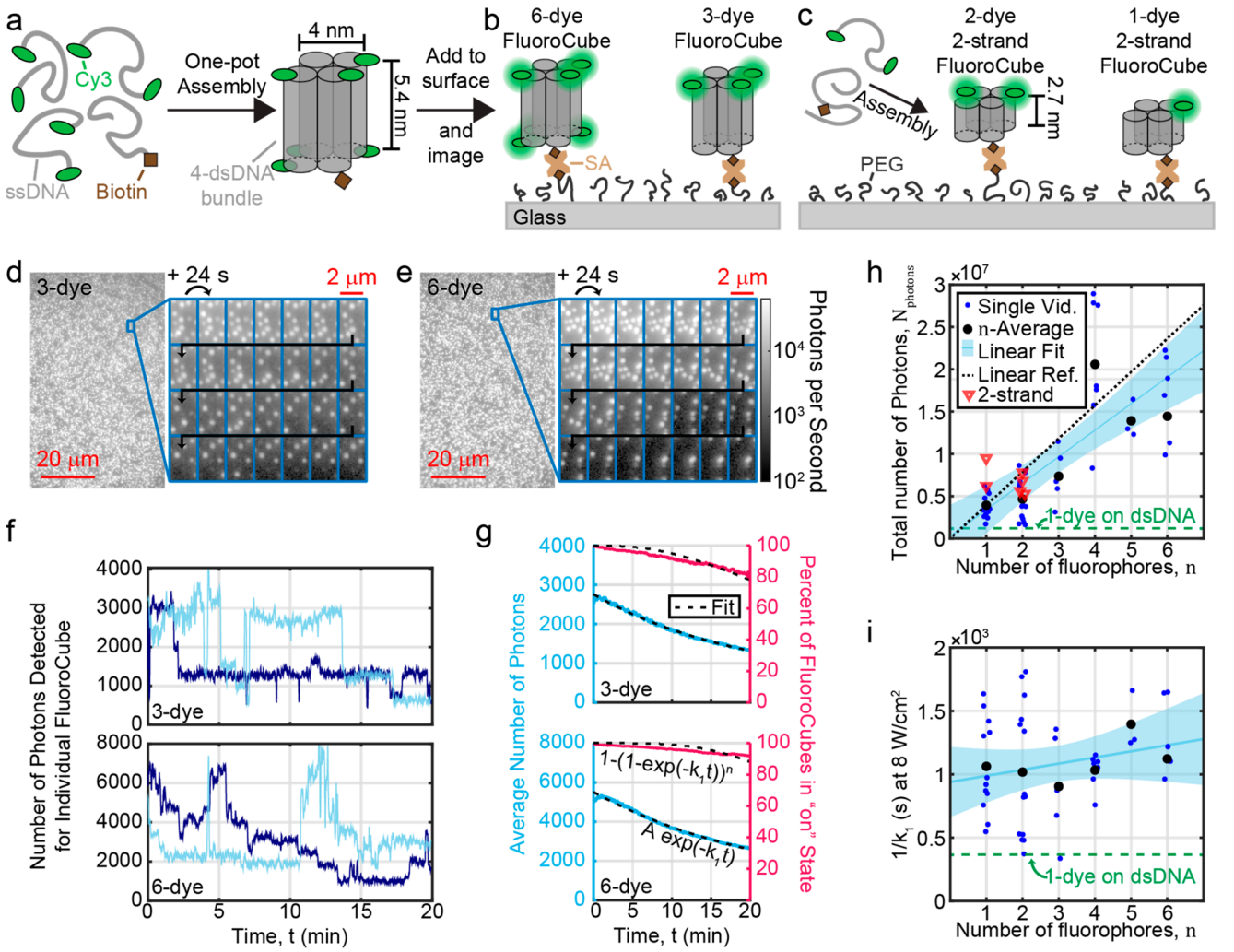

Figure 1. Cy3 FluoroCube photostability arises from interactions between fluorophores and the DNA nanostructure. (a) Schematic depiction of fluorocube assembly from four oligonucleotides. (b) Depiction of FluoroCubes captured on a surface via a biotin−streptavidin linker. (c) Depiction of assembly and surface capture of miniature FluoroCubes assembled from two strands. (d) Initial frame from video of single molecule photobleaching of 3-dye FluoroCubes. A zoomed-in region is shown for 28 frames taken at 24 s intervals throughout the video. (e) Same as d, but for 6-dye FluoroCubes. Note the logarithmic scale of the intensity scale bar applicable to panels d and e. (f) Two representative photon count versus time traces each for 3-dye (top) and 6-dye (bottom) FluoroCubes. (g) Average photon count (left *y*-axis scale, blue curves) and percent of unbleached FluoroCubes (right *y*-axis scale, red curves) with dashed line fits (to eqs 1 and 2, respectively) for 3-dye (top) and 6-dye (bottom) FluoroCubes. (h) Plot summarizing $N_{photons}$ versus n for 14 fluorocube constructs, showing roughly linear scaling. Blue curve and shading show best-fit and 95% confidence interval of the linear fit. Horizontal green dashed line indicates $N_{photons}$ for a single Cy3 dye attached to a double-stranded DNA duplex. Blue dots show best-fit values from individual videos of standard 4-strand FluoroCube photobleaching. Black dots show average of all best-fit values at a given n. Red triangles show best-fit values from individual videos of 2-strand FluoroCube photobleaching. Black dotted line passes through the origin and the 1-dye average value. (i) Same as h, but for $1/k_1$ (normalized to a common excitation laser power density), showing no significant correlation with n.

$$f = 1 - (1 - \exp(-k_1 t))^n \quad (2)$$

Fitting to both eqs 1 and 2 produced similar results (Figure S5).

Although $N_{photons}$ correlated significantly with n ($p < 0.001$, Figure 1h), k_1 did not ($p = 0.14$, Figure 1i). In other words, the photostability of FluoroCube-bound Cy3 dyes is independent of the number of other dyes on the FluoroCube. Contrary to our original hypothesis, this finding shows that photostabilization is primarily the result of interactions between individual dyes and the DNA nanostructures they are linked to − not dye−dye interactions.

Why then did the aforementioned measurement with increased dye−dye spacings (≥8 nm) exhibit ∼2× lower τ and $N_{photons}$?[13] Upon further inspection, we found that Cy3 dyes were attached to the larger cube nanostructure via 2T overhangs, which could have partially disrupted dye−DNA interactions and thus reduced photstability.[27] Similar overhangs were not used to attach dyes to FluoroCubes, highlighting the importance and sensitivity of dye−DNA interactions in photostabilization.

Our conclusions suggest that FluoroCube size can be further reduced, so long as dye−DNA interactions are preserved. To test this hypothesis, we designed 1-dye and 2-dye FluoroCubes composed of only two strands with approximate dimensions of 4.0 × 4.0 × 2.7 nm^3 (assuming a duplex width of 2 nm and length of ∼0.34 nm per basepair, see Figures 1c,h and S3). To relieve internal strain within this nanostructure, we added 2T or 4T loops (both appear to work equally well, Figure S3) to

https://doi.org/10.1021/acs.nanolett.2c01757
Nano Lett. 2022, 22, 6235−6244

each of the three duplex crossovers. These 2-strand FluoroCubes appeared to emit slightly more photons than full-size 4-strand 1- and 2-dye FluoroCubes, although the two constructs were imaged using different microscopes (p = 0.033 and p = 0.015, respectively, Figures S3 and S6). These 2-strand FluoroCubes have a similar volume (~45 nm^3) to minimal green fluorescent protein (~36 nm^3),[35] and could potentially be loaded with additional fluorophores via modification of internal sites and the remaining unused strand terminus.

As a control, we performed single molecule photobleaching studies of single Cy3 dyes attached to surface-captured double-stranded DNA (dsDNA; Figure 1h,i). We were able to collect 4× as many photons (1.2 million) per Cy3 dye than reported in the previous work on FluoroCubes[13] (0.3 million). As a result, the 6-dye FluoroCube to 1-dye DNA duplex ratios of photobleaching half-life and total photon count are lower in this work (6.4 ± 0.5× and 12.3 ± 0.6×, respectively) than originally reported[13] (54× and 43×, respectively). (The photobleaching half-life ratio was calculated by multiplying the ratio of k_1 values, 2.9, by 1.13ln(7) − see Supporting Information Note 1). Our ratios are therefore in line with the enhancements reported in the same prior work[13] for dyes other than Cy3. The discrepancy between our work and the previous study may lie in slight differences between buffer conditions, purification strategies, and imaging systems.

$N_{photons}/n$ did not scale significantly with n (p = 0.069), suggesting a linear increase in brightness with n. However, this result appeared to be influenced by the high $N_{photons}$ exhibited by 4-dye FluoroCubes (which was indistinguishable from that of 6-dye FluoroCubes, p = 0.38). (Increased aggregation was not the source of the high brightness for 4-dye FluoroCubes, Supporting Information Note 2). For $n \neq 4$, $N_{photons}$ scaled sublinearly with n ($p < 0.001$) on-surface (Figure S6), and brightness scaled sublinearly in bulk solution (Figure S7). This suggests that dye−dye interactions such as H-dimerization and singlet−singlet annihilation may actually negatively impact FluoroCube performance by reducing $N_{photons}$.[33,36,37]

To assess the role of dye−dye interactions in FluoroCube performance, we performed statistical comparisons between our single molecule photobleaching measurements. For these comparisons, FluoroCube constructs were grouped according to interdye spacing (for 2-dye Fluorocubes) and n (Figure S8−9, Supporting Information Note 3). While we observed differences in I_0 and $N_{photons}$ as a function of n, these quantities did not differ between 2-dye constructs as a function of interdye spacing. (Few differences in k_1 were observed between constructs). Accordingly, we sought an alternative approach for assessing the role of dye−dye interactions.

Nonfluorescent face-to-face Cy3 H-dimers can be detected via the presence of a large blue-shifted peak[13,32,38] in the Cy3 absorbance spectrum. We measured absorbance spectra of all 14 FluoroCube constructs (Figures 2a,b, S10) and observed H-dimerization in four: 2-dye AB, 3-dye ABC, 5-dye ABC-AC, and 6-dye ABC-ABC. These four constructs (which we call "+H") collectively exhibited significantly fewer $N_{photons}/n$ (photons detected per dye) than the ten other, low H-dimerization constructs (which we call "-H", Figures 2c, S11). None of these constructs were fully quenched, suggesting that H-dimerization is imperfect (i.e., dyes continuously transition between dimeric and monomeric states).[37] The +H and -H groups showed no significant difference in k_1 (Figures 2d, S11), suggesting that H-dimerization does not alter photobleaching kinetics.

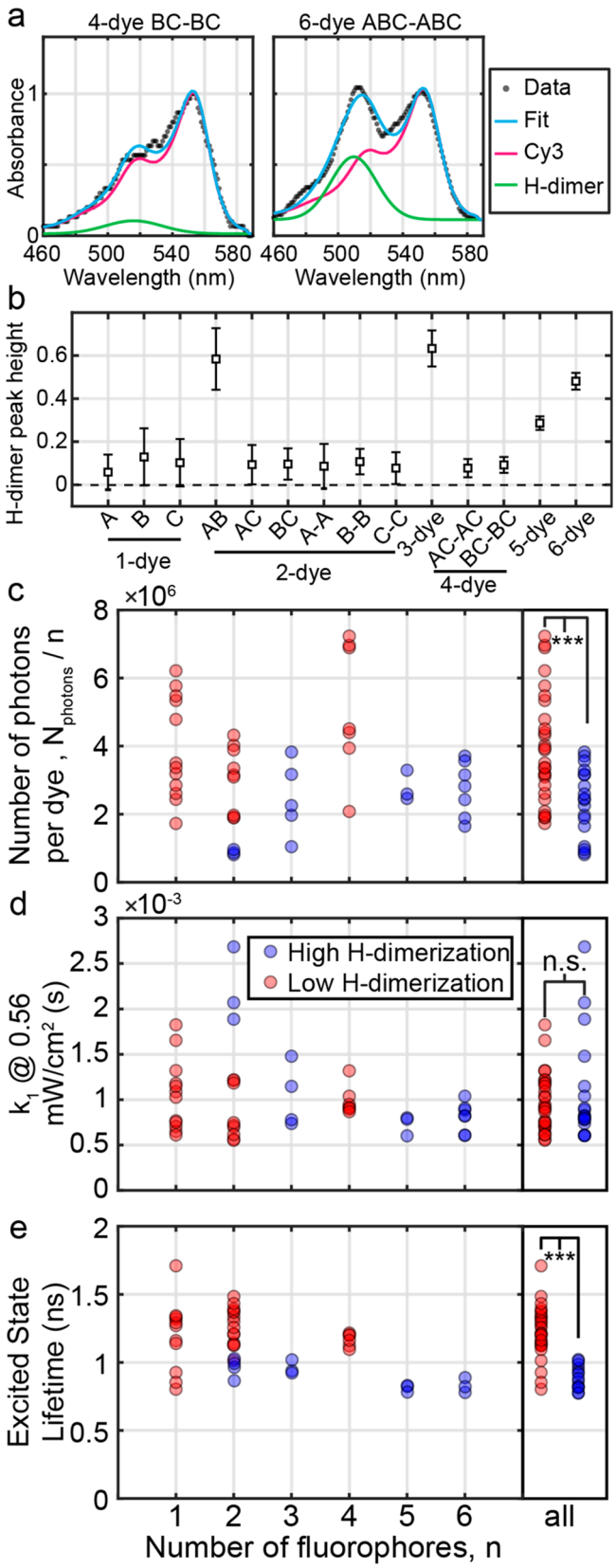

Figure 2. H-dimerization can perturb FluoroCube function. (a) Representative absorbance spectra of 4-dye BC-BC (left) and 6-dye ABC-ABC FluoroCubes. A curve fit, consisting of a Cy3 spectrum plus an H-dimer peak centered on ~515 nm (see Figure S10 for more information) is shown in cyan. The two components of the curve fit are shown in magenta and green. (b) The height of the H-dimer component of the absorbance spectrum fit (best fit ± 95% confidence

https://doi.org/10.1021/acs.nanolett.2c01757
Nano Lett. 2022, 22, 6235−6244

Figure 2. continued

interval of the fit), normalized to the height of the Cy3 spectrum component, is shown for each of the 14 constructs studied in this work. Four constructs (2-dye AB, 3-dye ABC, 5-dye ABC-AC, and 6-dye ABC-ABC) stand out as exhibiting heightened levels of H-dimerization. (c−e) Scattered points showing individual measurements of $N_{photons}/n$ (c), k_1 (d), and the excited state fluorescence lifetime (e) measured as a function of n. Red and blue scatter points show -H and +H FluoroCubes, respectively. Two-sided t tests comparing all constructs in high and low H-dimerization groups (right side of each plot) showed that the +H constructs emit fewer total photons per dye and have shorter excited state lifetimes than their -H counterparts yet exhibit the same rate of photobleaching (*** denotes $p < 0.001$, n.s. denotes $p > 0.05$).

The intensity of single +H FluoroCubes fluctuated significantly more than -H FluoroCubes (Figure S12). We ascribe this observation to the increased number of discrete brightness levels that are possible when dyes can exist in (and transition between) monomeric and dimeric states. The 4-dye FluoroCubes exhibited the fewest intensity fluctuations of all constructs. Altogether, reducing n from six to four significantly reduces intensity fluctuations without compromising total photon count, brightness, or photostability—thus representing an overall improvement in performance at reduced cost.

We noticed that H-dimerization only occurred in constructs with a pair (or two pairs) of dyes that were 1) on adjacent duplexes, and 2) both attached to a terminal A-T pair. Cyanine dyes are known to stack against the termini of the DNA duplexes they are coupled to, and the energy of stacking to a terminal G-C is ∼2−4 kcal/mol higher than stacking to a terminal A-T.[39] Therefore, it appears that H-dimerization may only occur when two fluorophores are close (within ∼2 nm) and are both unstacked from their respective DNA duplex termini. Perhaps in future work, FluoroCube performance can be improved by strategically mutating terminal basepairs to limit H-dimerization. It is also possible that other local structural factors are responsible for these differences.

We also measured the excited-state fluorescence lifetimes (Figures 2e, S13a, and S14) and time-resolved fluorescence anisotropies (Figure S13b) of our 14 constructs. The fluorescence lifetime was significantly shorter for +H constructs than -H constructs ($p < 0.001$), and correlated negatively with n for +H constructs ($p < 0.01$) but not -H constructs ($p = 0.74$). Decreased excited state lifetime is a hallmark of fluorescence quenching and H-dimerization due to increased competition between radiative and nonradiative energy decay pathways. Fluorescence anisotropy negatively correlated with n, which we attribute to FRET between Cy3 dyes (homoFRET, Figures S15 and S16). While homoFRET alone is not expected to reduce FluoroCube brightness, its presence suggests that singlet−singlet annihilation (which reduces brightness at high laser power via a similar process to homoFRET) may occur. Consistent with this expectation (and with prior work[13]), brightness/n was negatively correlated with n at high laser powers (Figure S15). See Supporting Information Note 4 for additional discussion of homoFRET and annihilation.

We next tested the compatibility of FluoroCubes with dark quenchers. Previous work has shown that unstructured DNA oligonucleotides (∼15 nt in length) flanked by fluorophore-quencher pairs exhibit high fluorogenicity (i.e., their brightness strongly increases upon hybridization to a complementary oligonucleotide, Figure 3a).[22,23] To apply this principle to FluoroCubes, we appended a 15 nt single-stranded overhang with a terminal black hole quencher (BHQ-2) to a 6-dye FluoroCube (Figure 3b), expecting that the BHQ-2 would form a ground-state complex with (and thus quench) the Cy3 dyes on the same face as the overhang (Figure 3a). To assess quenching efficiency, we measured in-solution fluorescence intensity before and after the addition of a complement strand, which hybridizes to the overhang and thus separates the quencher from the Cy3 dyes.[22,23]

The 6-dye fluorogenic FluoroCube's fluorescence increased by ∼60% following hybridization, (Figure 3b). For reference, the overhang strand alone flanked by Cy5 and BHQ-2 exhibited a ∼20×, or 2,000%, increase (Figure 3a). We hypothesized that the lower fluorogenicity of the 6-dye FluoroCube could be explained by moderate quenching of the three fluorophores on the same face as the overhang and inefficient quenching of the three fluorophores on the opposite face. To test this hypothesis, we designed two 3-dye FluoroCubes: one with three fluorophores on the same side as the quencher overhang (*cis*, Figures 3c and S17b), and one with three fluorophores on the opposite side (*trans*, Figure 3d and S17b). The 3-dye *cis*- and *trans*-FluoroCubes exhibited 400% and 25% increases in fluorescence upon hybridization, respectively (Figure 3c,d). The 400% increase for the 3-dye *cis* FluoroCube corresponds to an 80% quenching efficiency.

To determine whether the quenching efficiency could be increased beyond 80%, we assembled and tested six additional *cis* FluoroCube constructs (Figure S17). Specifically, we designed three 1-dye *cis* Fluorocube constructs, each with a fluorophore in one of three positions (denoted A, B, and C as shown in Figure 3e) and three 2-dye *cis* Fluorocube constructs, each with two fluorophores in a unique combination of those positions. The 1-dye A, 1-dye B, and 2-dye AB constructs all exhibited a ∼ 50% quenching efficiency, which was significantly lower than that of the 3-dye *cis*-FluoroCube ($p < 0.01$, Figure 3e). However, the 1-dye C, 2-dye AC, and 2-dye BC constructs each exhibited enhanced (85−90%) quenching efficiencies, which were significantly higher than that of the 3-dye *cis*-FluoroCube construct ($p < 0.01$, Figure 3e).

To summarize, quenching efficiency appears to be maximized when a fluorophore is in position C and there are either no additional fluorophores or one fluorophore in either position A or position B (but not both). The site dependence of fluorogenicity is likely the result of localized properties such as linkage strategy, DNA sequence, and H-dimerization.[13,40] Such local properties, as well as localized properties of neighboring dyes, likely affect the extent to which the quencher can interact with the dye. As pointed out in the section on H-dimerization, the dye in the C-position is flanked immediately by a C-G pair, while the A- and B-position dyes are flanked by A-T pairs (Table S1). Accordingly, the C-position dye could be expected to spend more time directly stacked against its duplex's terminus.[39] Conversely, the A- and B-position dyes are bound to less thermodynamically stable duplex termini, and thus may spend more time in an unstacked state due to duplex "breathing".[41] Perhaps the DNA-stacked fluorophore at the C-position is more readily available for contact quenching by BHQ-2 than the unstacked fluorophores at the A- and B-positions and, following recruitment to the C-position, the quencher can efficiently quench one additional unstacked fluorophore.

https://doi.org/10.1021/acs.nanolett.2c01757
Nano Lett. 2022, 22, 6235−6244

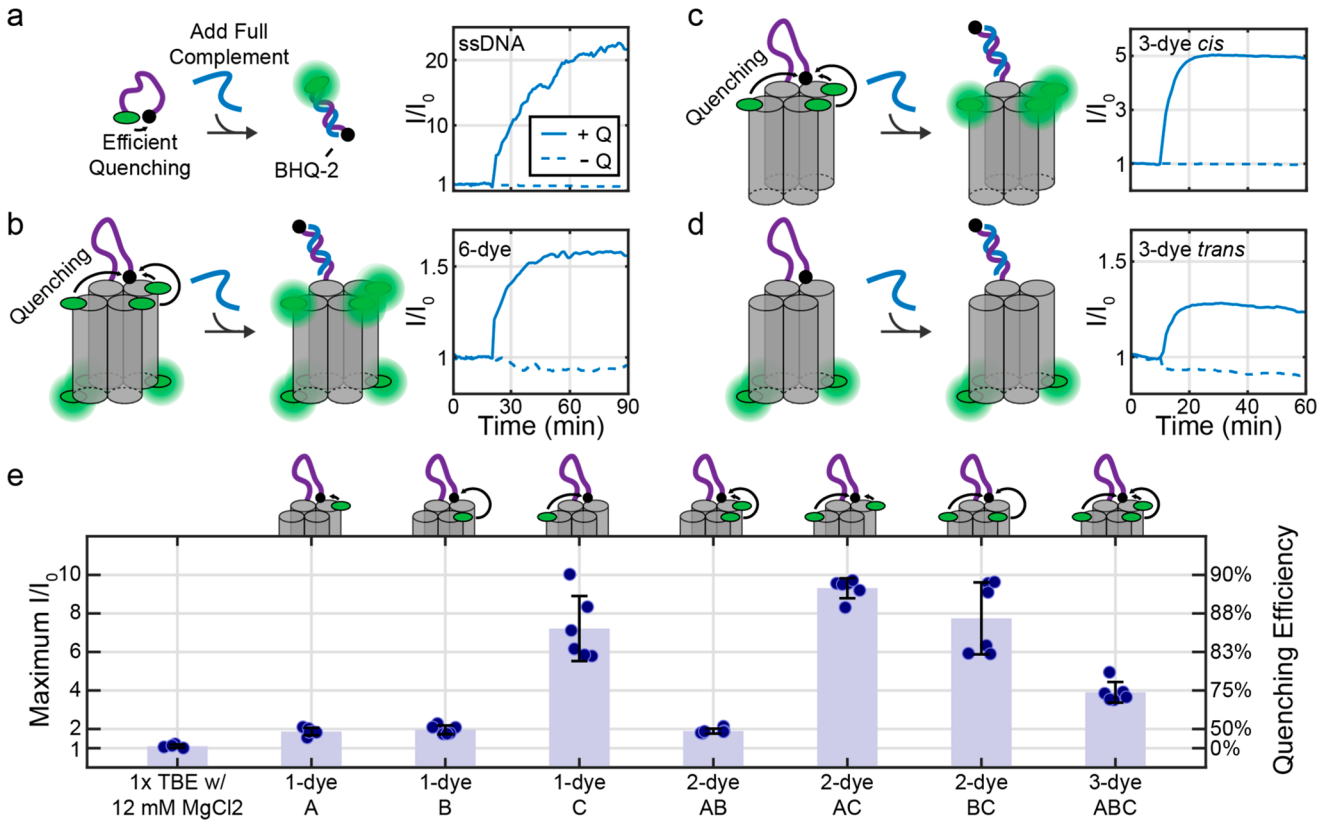

Figure 3. FluoroCubes are compatible with dark quenching applications. (a) Schematic of single-stranded 15 nt fluorogenic DNA exhibiting dequenching upon hybridization to a full complement (left) and in-solution normalized fluorescence intensity before and after equimolar addition of a full complement oligonucleotide in 4× PBS (right). (b–d) Same as panel a, but for 6-dye, 3-dye *cis*, and 3-dye *trans* FluoroCubes in 1× TBE with 12 mM $MgCl_2$. Note that all four plots in a–d have different *y*-axis scales and have dashed curves showing the results of control experiments performed in the absence of BHQ-2 quenchers. (e) Maximum in-solution normalized fluorescence intensity from seven 1-, 2-, and 3-dye *cis* FluoroCube constructs, as well as a FluoroCube-free control. Circles show individual data points from six experimental replicates, whereas bars and errorbars show average and standard deviation of replicates. The right *y*-axis shows the quenching efficiency at each grid line.

Finally, we examined whether FluoroCubes could be used in FRET applications. Via one-pot assembly, we coassembled a 6-dye Cy3 FluoroCube (donor) and a 6-dye Cy5 FluoroCube (acceptor) attached via complementary single-stranded DNA overhangs (Figure 4a). We also performed the same assembly in the presence of excess "separator" strand, which binds to the Cy5 FluoroCube's overhang more stably (21 bp) than the Cy3 FluoroCube's overhang does (15 bp). (The separator can also displace the Cy3 FluoroCube's overhang through toehold-mediated strand displacement.) We then performed agarose gel electrophoresis for 3 h post assembly and imaged the gel to measure the effective FRET efficiency (E_{eff}, an imperfect quantifier of FRET that is proportional to the concentration of donor–acceptor complex, Figures 4b,c, and S18). In the absence of the separator, a low mobility band (assembled complex) exhibited high E_{eff} (Figure 4b–d). In the presence of the separator, the low mobility band disappeared and was replaced by higher mobility bands (individual FluoroCubes), which exhibited low E_{eff} (Figure 4b–d). When the separator and all six dyes on the Cy3 FluoroCube were removed, the low mobility band was recovered, but the E_{eff} of this band remained low (Figure 4b–d). Similar results were observed when using a 3-dye *cis* Cy3 FluoroCube, and with 3- and 6-dye Cy3 fluorogenic FluoroCubes (Figure S19). These results demonstrate that FluoroCubes are compatible with FRET applications.

The current work presents evidence that Cy3 FluoroCube ultraphotostability arises from dye–DNA interactions, rather than dye–dye interactions. We expect that the same is true for FluoroCubes with other dyes, particularly structural analogs like Cy5. Cy3 is known to photobleach through two parallel pathways: isomerization and photo-oxidation.[42] The four-helix bundle may inhibit isomerization by interacting through stacking interactions[43] with the Cy3 and stabilizing the bright isomer.[7,27] The bundle may also inhibit photo-oxidation by excluding oxygen from the fluorophores' local environment or by altering the electronic structure of the dye's excited state[7] (as indicated by changes to Cy3 FluoroCubes' emission spectra[13]). Similar levels of photostabilization have been observed when Cy3 is attached internally to double stranded DNA[27] (and even proteins[44,45]), suggesting that the presence of multiple bundled DNA duplex termini further compound such effects. For future work, this interpretation naturally raises important questions: How much further can photostability be enhanced by attaching dyes to larger DNA bundles or labeling them internally, deep within dense DNA origami nanostructures? Do bundled DNA nanostructures generally confer stabilization to certain fluorophores? Recent work has shown that fluorophores can interact with DNA nanotechnology through a variety of interactions modes (e.g., base stacking, groove binding, binding to crossovers) that are highly sensitive to attachment chemistry and local DNA environment.[46] Some of these interactions are unique to multihelix structural motifs.

https://doi.org/10.1021/acs.nanolett.2c01757
Nano Lett. 2022, 22, 6235–6244

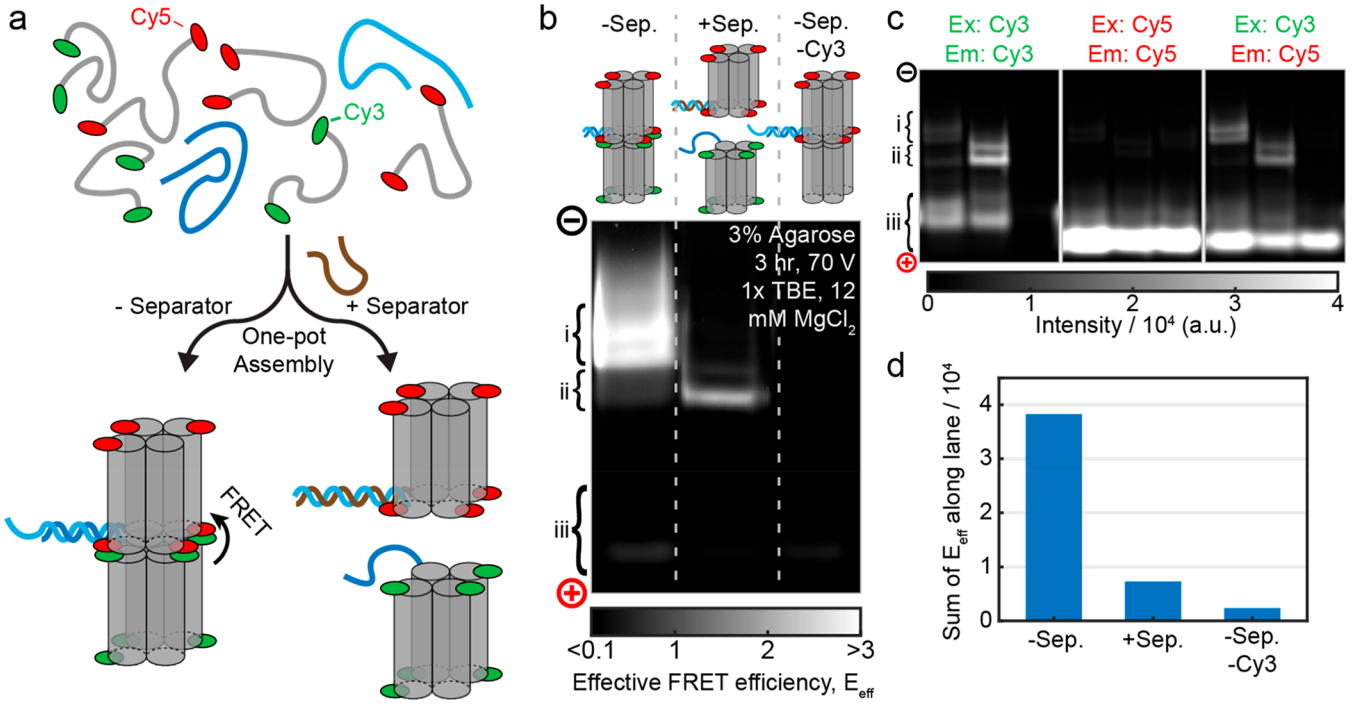

Figure 4. FluoroCubes are compatible with FRET applications. (a) Schematic depiction of the one-pot assembly of Cy3-Cy5 FluoroCube complexes from eight strands (left) or separated FluoroCubes with the addition of a separator strand. (b) Image of the effective FRET efficiency, E_{eff}, of single and complexed FluoroCubes in a 3% agarose gel after 3 h of gel electrophoresis. (c) The raw images used to calculate E_{eff} (the lanes are the same as in (b)). Gel images are labeled on the left with a + and − end showing that the electrophoretic direction was from top (−) to bottom (+) in the image. Curly brackets show the approximate coordinates that were generally interpreted as containing assembled FluoroCube complexes (i), individual FluoroCubes (ii), or incomplete FluoroCubes and unassembled single strands (iii). We expect that the presence of multiple bands in ii and iii is the result of end-to-end stacking between FluoroCubes. (d) Integrated E_{eff} for the three lanes (this is mathematically valid because E_{eff} is proportional to the concentration of FRET complex) showing very high FRET for only the complexed FluoroCubes with both Cy3 and Cy5 dyes.

We find it likely that single molecule photobleaching studies of existing DNA-based technologies[47,48] may reveal photostability that exceeds what has already been shown.

Dye−dye interactions, on the other hand, appear to undermine FluoroCube quality.[37] Our work suggests that 4-dye FluoroCubes may be optimal, potentially because they best balance the trade-off between having increased brightness due to increased n and an increase in self-quenching interactions due to crowding of fluorophores into a small space. Four-dye FluoroCubes also benefit from having two additional free DNA termini that can be labeled with useful chemical tags such as triplet state quenchers,[49] photoprotective agents,[50] and targeting motifs.[51] Even four-dye FluoroCubes will likely suffer from brightness reduction at very high laser powers due to singlet−singlet annihilation. However, the control and programmability offered by DNA nanotechnology suggests that similar processes with desirable outcomes − such as triplet−triplet annihilation for photon upconversion − could be rationally engineered using FluoroCube-like technologies.[52]

This work also demonstrates that FluoroCubes are compatible with FRET and dark quenching applications. Extension of these principles to single molecule applications could enable high signal-to-noise studies of molecular conformational dynamics with unprecedented duration (>1 h).[15,53] The high photostability of individual FluoroCubes, even in the absence of OSS (FluoroCubes without OSS have comparable photostability to individual fluorophores with OSS[13]) could allow such studies, typically performed on purified biochemicals conjugated to glass, to be performed within living cells and other more complex systems. The similarity in size between FluoroCubes (particularly miniature 2-strand FluoroCubes) and genetically encoded fluorescent proteins speaks to the feasibility of such techniques. Cytosolic delivery of FluoroCubes is a challenge that may necessitate microinjection or plasma membrane permeabilization.[54] Susceptibility to nuclease degradation is also a potential concern, although it is also possible that, similar to other DNA nanostructures, FluoroCubes exhibit increased resistance to nucleases.[55]

The tight packing of dyes on a FluoroCube enables simultaneous quenching of multiple fluorophores by a single dark quencher (Figure 3). The maximum quenching efficiency of ∼90% can potentially be improved further with the use of multiple quenchers[56] and/or sequence refinement. Fluorogenic FluoroCubes are likely compatible with existing techniques such as molecular tension fluorescence microscopy[24,25,57−60] and fluorogenic DNA PAINT.[22] Because dark quenchers are known to shield fluorophores from photobleaching,[61] fluorogenic FluoroCubes may one day enable DNA PAINT[22,60,62] and kinetic fingerprinting-type[19,63,64] applications in which the imagers are under constant illumination, confined to fixed compartments (e.g., live cells) without the ability to exchange with the surrounding environment.

■ ASSOCIATED CONTENT

Supporting Information

The Supporting Information is available free of charge at https://pubs.acs.org/doi/10.1021/acs.nanolett.2c01757.

https://doi.org/10.1021/acs.nanolett.2c01757
Nano Lett. 2022, 22, 6235−6244

Experimental and computational methods, supplemental Figures S1−S19, supplemental Tables 1−2, and supplemental Notes 1−4 (PDF)

AUTHOR INFORMATION

Corresponding Author

Nils G. Walter − *Single Molecule Analysis Group, Department of Chemistry and Center for RNA Biomedicine, University of Michigan, Ann Arbor, Michigan 48109, United States;* orcid.org/0000-0002-7301-1275; Email: nwalter@umich.edu

Authors

Aaron T. Blanchard − *Single Molecule Analysis Group, Department of Chemistry, Department of Biomedical Engineering, and Michigan Society of Fellows, University of Michigan, Ann Arbor, Michigan 48109, United States;* Present Address: Department of Biomedical Engineering, Duke University, Durham, North Carolina, 27705, United States; orcid.org/0000-0002-3129-6591

Zi Li − *Single Molecule Analysis Group, Department of Chemistry, University of Michigan, Ann Arbor, Michigan 48109, United States;* Present Address: Pacific Biosciences, Menlo Park, California, 94025, United States.

Elizabeth C. Duran − *Single Molecule Analysis Group, Department of Chemistry, University of Michigan, Ann Arbor, Michigan 48109, United States*

Catherine E. Scull − *Single Molecule Analysis Group, Department of Chemistry, University of Michigan, Ann Arbor, Michigan 48109, United States*

J. Damon Hoff − *Single Molecule Analysis in Real-Time (SMART) Center, University of Michigan, Ann Arbor, Michigan 48109, United States*

Keenan R. Wright − *Department of Chemistry, University of Michigan, Ann Arbor, Michigan 48109, United States*

Victor Pan − *Department of Biomedical Engineering, Emory University and the Georgia Institute of Technology, Atlanta, Georgia 30322;* Present Address: Intellia Therapeutics, Cambridge, Massachusetts 02139, United States.

Complete contact information is available at: https://pubs.acs.org/10.1021/acs.nanolett.2c01757

Author Contributions

All authors have given approval to the final version of the manuscript.

Notes

The authors declare no competing financial interest.

ACKNOWLEDGMENTS

We acknowledge use of the Single Particle Tracker equipment in the Single Molecule Analysis in Real-Time (SMART) Center at the University of Michigan, seeded by NSF MRI-ID grant DBI-0959823. We thank Viktorjia Glembockyte and Philip Tinnefeld (LMU Munich) for helpful conversations. This work was supported by the United States National Institutes of Health (NIH) in the form of Grants R35 GM131922, R21 CA204560, and R33 CA229023 to N.G.W., F32 GM140547 to C.E.S., NIH IRACDA fellowship Grant K12 GM111725 to E.C.D., and K00 CA245789 to A.T.B..

ABBREVIATIONS

DNA, deoxyribonucleic acid; FRET, Förster resonance energy transfer; SA, streptavidin; Cy3, cyanine 3; Cy5, cyanine 5; BHQ-2, black hole quencher 2; OSS, oxygen scavenging system; PAINT, points accumulation for imaging in nanoscale topology; PEG, poly(ethylene glycol); PCA, protocatechuic acid; PCD, protocatechuate-3,4-dioxygenase

REFERENCES

(1) Zheng, Q.; Juette, M. F.; Jockusch, S.; Wasserman, M. R.; Zhou, Z.; Altman, R. B.; Blanchard, S. C. Ultra-stable organic fluorophores for single-molecule research. *Chem. Soc. Rev.* **2014**, *43* (4), 1044−1056.

(2) Renikuntla, B. R.; Rose, H. C.; Eldo, J.; Waggoner, A. S.; Armitage, B. A. Improved Photostability and Fluorescence Properties through Polyfluorination of a Cyanine Dye. *Org. Lett.* **2004**, *6* (6), 909−912.

(3) Toutchkine, A.; Nguyen, D.-V.; Hahn, K. M. Merocyanine Dyes with Improved Photostability. *Org. Lett.* **2007**, *9* (15), 2775−2777.

(4) Aitken, C. E.; Marshall, R. A.; Puglisi, J. D. An Oxygen Scavenging System for Improvement of Dye Stability in Single-Molecule Fluorescence Experiments. *Biophys. J.* **2008**, *94* (5), 1826−1835.

(5) Rasnik, I.; McKinney, S. A.; Ha, T. Nonblinking and long-lasting single-molecule fluorescence imaging. *Nat. Methods* **2006**, *3* (11), 891−893.

(6) Glembockyte, V.; Lincoln, R.; Cosa, G. Cy3 Photoprotection Mediated by Ni2+ for Extended Single-Molecule Imaging: Old Tricks for New Techniques. *J. Am. Chem. Soc.* **2015**, *137* (3), 1116−1122.

(7) Glembockyte, V.; Frenette, M.; Mottillo, C.; Durantini, A. M.; Gostick, J.; Štrukil, V.; Friščić, T.; Cosa, G. Highly Photostable and Fluorescent Microporous Solids Prepared via Solid-State Entrapment of Boron Dipyrromethene Dyes in a Nascent Metal−Organic Framework. *J. Am. Chem. Soc.* **2018**, *140* (49), 16882−16887.

(8) Guether, R.; Reddington, M. V. Photostable Cyanine Dye β-Cyclodextrin Conjugates. *Tetrahedron Lett.* **1997**, *38* (35), 6167−6170.

(9) Yau, C. M. S.; Pascu, S. I.; Odom, S. A.; Warren, J. E.; Klotz, E. J. F.; Frampton, M. J.; Williams, C. C.; Coropceanu, V.; Kuimova, M. K.; Phillips, D.; Barlow, S.; Brédas, J.-L.; Marder, S. R.; Millar, V.; Anderson, H. L. Stabilisation of a heptamethine cyanine dye by rotaxane encapsulation. *Chem. Commun.* **2008**, No. 25, 2897−2899.

(10) Yang, S. K.; Shi, X.; Park, S.; Ha, T.; Zimmerman, S. C. A dendritic single-molecule fluorescent probe that is monovalent, photostable and minimally blinking. *Nat. Chem.* **2013**, *5* (8), 692−697.

(11) Mohanty, J.; Nau, W. M. Ultrastable Rhodamine with Cucurbituril. *Angew. Chem., Int. Ed.* **2005**, *44* (24), 3750−3754.

(12) Chen, M.; Yin, M. Design and development of fluorescent nanostructures for bioimaging. *Prog. Polym. Sci.* **2014**, *39* (2), 365−395.

(13) Niekamp, S.; Stuurman, N.; Vale, R. D. A 6-nm ultra-photostable DNA FluoroCube for fluorescence imaging. *Nat. Methods* **2020**, *17* (4), 437−441.

(14) Niekamp, S.; Stuurman, N.; Zhang, N.; Vale, R. D. Three-color single-molecule imaging reveals conformational dynamics of dynein undergoing motility. *Proc. Natl. Acad. Sci. U. S. A.* **2021**, *118* (31), e2101391118.

(15) Sasmal, D. K.; Pulido, L. E.; Kasal, S.; Huang, J. Single-molecule fluorescence resonance energy transfer in molecular biology. *Nanoscale* **2016**, *8* (48), 19928−19944.

(16) Pehlivan, Z. S.; Torabfam, M.; Kurt, H.; Ow-Yang, C.; Hildebrandt, N.; Yüce, M. Aptamer and nanomaterial based FRET biosensors: a review on recent advances (2014−2019). *Microchimica Acta* **2019**, *186* (8), 563.

(17) Rowland, C. E.; Brown, C. W.; Medintz, I. L.; Delehanty, J. B. Intracellular FRET-based probes: a review. *Methods and applications in fluorescence* **2015**, *3* (4), 042006.

(18) Ham, T. R.; Collins, K. L.; Hoffman, B. D. Molecular tension sensors: moving beyond force. *Current Opinion in Biomedical Engineering* **2019**, *12*, 83−94.
(19) Khanna, K.; Mandal, S.; Blanchard, A. T.; Tewari, M.; Johnson-Buck, A.; Walter, N. G. Rapid kinetic fingerprinting of single nucleic acid molecules by a FRET-based dynamic nanosensor. *Biosens. Bioelectron.* **2021**, *190*, 113433.
(20) Ryazantsev, D. Y.; Kvach, M. V.; Tsybulsky, D. A.; Prokhorenko, I. A.; Stepanova, I. A.; Martynenko, Y. V.; Gontarev, S. V.; Shmanai, V. V.; Zavriev, S. K.; Korshun, V. A. Design of molecular beacons: 3′ couple quenchers improve fluorogenic properties of a probe in real-time PCR assay. *Analyst* **2014**, *139* (11), 2867−2872.
(21) Zheng, J.; Yang, R.; Shi, M.; Wu, C.; Fang, X.; Li, Y.; Li, J.; Tan, W. Rationally designed molecular beacons for bioanalytical and biomedical applications. *Chem. Soc. Rev.* **2015**, *44* (10), 3036−3055.
(22) Chung, K. K. H.; Zhang, Z.; Kidd, P.; Zhang, Y.; Williams, N. D.; Rollins, B.; Yang, Y.; Lin, C.; Baddeley, D.; Bewersdorf, J. Fluorogenic probe for fast 3D whole-cell DNA-PAINT. *Nature Methods* **2022**, *19*, 554−559.
(23) Kashida, H.; Morimoto, K.; Asanuma, H. A stem-less probe using spontaneous pairing between Cy3 and quencher for RNA detection. *Sci. Technol. Adv. Mater.* **2016**, *17* (1), 267−273.
(24) Zhang, Y.; Ge, C.; Zhu, C.; Salaita, K. DNA-based digital tension probes reveal integrin forces during early cell adhesion. *Nat. Commun.* **2014**, *5*, 5167.
(25) Brockman, J. M.; Blanchard, A. T.; Pui-Yan Ma, V.; Derricotte, W. D.; Zhang, Y.; Fay, M. E.; Lam, W. A.; Evangelista, F. A.; Mattheyses, A. L.; Salaita, K. Mapping the 3D orientation of piconewton integrin traction forces. *Nat. Methods* **2018**, *15*, 115.
(26) Marras, S. A. E. Efficiencies of fluorescence resonance energy transfer and contact-mediated quenching in oligonucleotide probes. *Nucleic Acids Res.* **2002**, *30* (21), 122e.
(27) Lee, W.; von Hippel, P. H.; Marcus, A. H. Internally labeled Cy3/Cy5 DNA constructs show greatly enhanced photo-stability in single-molecule FRET experiments. *Nucleic Acids Res.* **2014**, *42* (9), 5967−5977.
(28) Pace, N. A.; Hennelly, S. P.; Goodwin, P. M. Immobilization of Cyanines in DNA Produces Systematic Increases in Fluorescence Intensity. *J. Phys. Chem. Lett.* **2021**, *12* (37), 8963−8971.
(29) Sorour, M. I.; Kistler, K. A.; Marcus, A. H.; Matsika, S. Accurate Modeling of Excitonic Coupling in Cyanine Dye Cy3. *J. Phys. Chem. A* **2021**, *125* (36), 7852−7866.
(30) Banal, J. L.; Kondo, T.; Veneziano, R.; Bathe, M.; Schlau-Cohen, G. S. Photophysics of J-Aggregate-Mediated Energy Transfer on DNA. *J. Phys. Chem. Lett.* **2017**, *8* (23), 5827−5833.
(31) Kringle, L.; Sawaya, N. P. D.; Widom, J.; Adams, C.; Raymer, M. G.; Aspuru-Guzik, A.; Marcus, A. H. Temperature-dependent conformations of exciton-coupled Cy3 dimers in double-stranded DNA. *J. Chem. Phys.* **2018**, *148* (8), 085101.
(32) Huff, J. S.; Davis, P. H.; Christy, A.; Kellis, D. L.; Kandadai, N.; Toa, Z. S. D.; Scholes, G. D.; Yurke, B.; Knowlton, W. B.; Pensack, R. D. DNA-Templated Aggregates of Strongly Coupled Cyanine Dyes: Nonradiative Decay Governs Exciton Lifetimes. *J. Phys. Chem. Lett.* **2019**, *10* (10), 2386−2392.
(33) Helmerich, D. A.; Beliu, G.; Sauer, M. Multiple-Labeled Antibodies Behave Like Single Emitters in Photoswitching Buffer. *ACS Nano* **2020**, *14* (10), 12629−12641.
(34) Saurabh, A.; Niekamp, S.; Sgouralis, I.; Pressé, S. Modeling Non-additive Effects in Neighboring Chemically Identical Fluorophores. *J. Phys. Chem. B* **2022**, *126*, 4216−4225, DOI: 10.1021/acs.jpcb.2c01889.
(35) Yang, F.; Moss, L. G.; Phillips, G. N. The molecular structure of green fluorescent protein. *Nat. Biotechnol.* **1996**, *14* (10), 1246−1251.
(36) Hofkens, J.; Cotlet, M.; Vosch, T.; Tinnefeld, P.; Weston, K. D.; Ego, C.; Grimsdale, A.; Müllen, K.; Beljonne, D.; Brédas, J. L.; Jordens, S.; Schweitzer, G.; Sauer, M.; De Schryver, F. Revealing competitive Förster-type resonance energy-transfer pathways in single bichromophoric molecules. *Proc. Natl. Acad. Sci. U. S. A.* **2003**, *100* (23), 13146.
(37) Schröder, T.; Scheible, M. B.; Steiner, F.; Vogelsang, J.; Tinnefeld, P. Interchromophoric Interactions Determine the Maximum Brightness Density in DNA Origami Structures. *Nano Lett.* **2019**, *19* (2), 1275−1281.
(38) Nicoli, F.; Roos, M. K.; Hemmig, E. A.; Di Antonio, M.; de Vivie-Riedle, R.; Liedl, T. Proximity-Induced H-Aggregation of Cyanine Dyes on DNA-Duplexes. *J. Phys. Chem. A* **2016**, *120* (50), 9941−9947.
(39) Spiriti, J.; Binder, J. K.; Levitus, M.; van der Vaart, A. Cy3-DNA stacking interactions strongly depend on the identity of the terminal basepair. *Biophys. J.* **2011**, *100* (4), 1049−1057.
(40) Kretschy, N.; Sack, M.; Somoza, M. M. Sequence-Dependent Fluorescence of Cy3- and Cy5-Labeled Double-Stranded DNA. *Bioconjugate Chem.* **2016**, *27* (3), 840−848.
(41) Jose, D.; Datta, K.; Johnson, N. P.; von Hippel, P. H. Spectroscopic studies of position-specific DNA "breathing" fluctuations at replication forks and primer-template junctions. *Proc. Natl. Acad. Sci. U. S. A.* **2009**, *106* (11), 4231.
(42) Jouonang, A. L.; Didier, P.; Mély, Y. Identification of a thermally activated process in the Cy3 photobleaching mechanism. *Phys. Chem. Chem. Phys.* **2012**, *14* (5), 1585−1588.
(43) Iqbal, A.; Arslan, S.; Okumus, B.; Wilson, T. J.; Giraud, G.; Norman, D. G.; Ha, T.; Lilley, D. M. J. Orientation dependence in fluorescent energy transfer between Cy3 and Cy5 terminally attached to double-stranded nucleic acids. *Proc. Natl. Acad. Sci. U. S. A.* **2008**, *105* (32), 11176.
(44) Rashid, F.; Raducanu, V.-S.; Zaher, M. S.; Tehseen, M.; Habuchi, S.; Hamdan, S. M. Initial state of DNA-Dye complex sets the stage for protein induced fluorescence modulation. *Nat. Commun.* **2019**, *10* (1), 2104.
(45) Lerner, E.; Ploetz, E.; Hohlbein, J.; Cordes, T.; Weiss, S. A Quantitative Theoretical Framework For Protein-Induced Fluorescence Enhancement−Förster-Type Resonance Energy Transfer (PIFE-FRET). *J. Phys. Chem. B* **2016**, *120* (26), 6401−6410.
(46) Hübner, K.; Joshi, H.; Aksimentiev, A.; Stefani, F. D.; Tinnefeld, P.; Acuna, G. P. Determining the In-Plane Orientation and Binding Mode of Single Fluorescent Dyes in DNA Origami Structures. *ACS Nano* **2021**, *15* (3), 5109−5117.
(47) Woehrstein, J. B.; Strauss, M. T.; Ong, L. L.; Wei, B.; Zhang, D. Y.; Jungmann, R.; Yin, P. Sub−100-nm metafluorophores with digitally tunable optical properties self-assembled from DNA. *Sci. Adv.* **2017**, *3* (6), e1602128.
(48) Pan, V.; Wang, W.; Heaven, I.; Bai, T.; Cheng, Y.; Chen, C.; Ke, Y.; Wei, B. Monochromatic Fluorescent Barcodes Hierarchically Assembled from Modular DNA Origami Nanorods. *ACS Nano* **2021**, *15*, 15892.
(49) Altman, R. B.; Terry, D. S.; Zhou, Z.; Zheng, Q.; Geggier, P.; Kolster, R. A.; Zhao, Y.; Javitch, J. A.; Warren, J. D.; Blanchard, S. C. Cyanine fluorophore derivatives with enhanced photostability. *Nat. Methods* **2012**, *9* (1), 68−71.
(50) Zheng, Q.; Jockusch, S.; Zhou, Z.; Altman, R. B.; Zhao, H.; Asher, W.; Holsey, M.; Mathiasen, S.; Geggier, P.; Javitch, J. A.; Blanchard, S. C. Electronic tuning of self-healing fluorophores for live-cell and single-molecule imaging. *Chemical Science* **2017**, *8* (1), 755−762.
(51) Lee, H.; Lytton-Jean, A. K. R.; Chen, Y.; Love, K. T.; Park, A. I.; Karagiannis, E. D.; Sehgal, A.; Querbes, W.; Zurenko, C. S.; Jayaraman, M.; Peng, C. G.; Charisse, K.; Borodovsky, A.; Manoharan, M.; Donahoe, J. S.; Truelove, J.; Nahrendorf, M.; Langer, R.; Anderson, D. G. Molecularly self-assembled nucleic acid nanoparticles for targeted in vivo siRNA delivery. *Nat. Nanotechnol.* **2012**, *7* (6), 389−393.
(52) Ahmad, W.; Wang, J.; Li, H.; Ouyang, Q.; Wu, W.; Chen, Q. Strategies for combining triplet−triplet annihilation upconversion sensitizers and acceptors in a host matrix. *Coord. Chem. Rev.* **2021**, *439*, 213944.

https://doi.org/10.1021/acs.nanolett.2c01757
Nano Lett. 2022, 22, 6235−6244

(53) Le Reste, L.; Hohlbein, J.; Gryte, K.; Kapanidis, A. N. Characterization of dark quencher chromophores as nonfluorescent acceptors for single-molecule FRET. *Biophys. J.* **2012**, *102* (11), 2658−2668.
(54) Balakrishnan, D.; Wilkens, G. D.; Heddle, J. G. Delivering DNA origami to cells. *Nanomedicine* **2019**, *14* (7), 911−925.
(55) Chandrasekaran, A. R. Nuclease resistance of DNA nanostructures. *Nature Reviews Chemistry* **2021**, *5* (4), 225−239.
(56) Hirotsu, Y.; Mochizuki, H.; Omata, M. Double-quencher probes improve detection sensitivity toward Severe Acute Respiratory Syndrome Coronavirus 2 (SARS-CoV-2) in a reverse-transcription polymerase chain reaction (RT-PCR) assay. *J. Virol. Methods* **2020**, *284*, 113926−113926.
(57) Dutta, P. K.; Zhang, Y.; Blanchard, A. T.; Ge, C.; Rushdi, M.; Weiss, K.; Zhu, C.; Ke, Y.; Salaita, K. Programmable Multivalent DNA-Origami Tension Probes for Reporting Cellular Traction Forces. *Nano Lett.* **2018**, *18* (8), 4803−4811.
(58) Zhang, Y.; Qiu, Y.; Blanchard, A. T.; Chang, Y.; Brockman, J. M.; Ma, V. P.-Y.; Lam, W. A.; Salaita, K. Platelet integrins exhibit anisotropic mechanosensing and harness piconewton forces to mediate platelet aggregation. *Proc. Natl. Acad. Sci. U. S. A.* **2018**, *115* (2), 325.
(59) Blanchard, A. T.; Salaita, K. Emerging uses of DNA mechanical devices. *Science* **2019**, *365* (6458), 1080−1081.
(60) Brockman, J. M.; Su, H.; Blanchard, A. T.; Duan, Y.; Meyer, T.; Quach, M. E.; Glazier, R.; Bazrafshan, A.; Bender, R. L.; Kellner, A. V.; Ogasawara, H.; Ma, R.; Schueder, F.; Peitrich, B. G.; Jungmann, R.; Li, R.; Mattheyses, A. L.; Ke, Y.; Salaita, K. Live-cell super-resolved PAINT imaging of pN cellular traction forces. *Nat. Methods* **2020**, *17* (10), 1018−1024.
(61) Ma, R.; Kellner, A. V.; Ma, V. P.-Y.; Su, H.; Deal, B. R.; Brockman, J. M.; Salaita, K. DNA probes that store mechanical information reveal transient piconewton forces applied by T cells. *Proc. Natl. Acad. Sci. U. S. A.* **2019**, *116* (34), 16949.
(62) Jungmann, R.; Avendaño, M. S.; Woehrstein, J. B.; Dai, M.; Shih, W. M.; Yin, P. Multiplexed 3D cellular super-resolution imaging with DNA-PAINT and Exchange-PAINT. *Nat. Methods* **2014**, *11* (3), 313−318.
(63) Johnson-Buck, A.; Su, X.; Giraldez, M. D.; Zhao, M.; Tewari, M.; Walter, N. G. Kinetic fingerprinting to identify and count single nucleic acids. *Nat. Biotechnol.* **2015**, *33* (7), 730−732.
(64) Chatterjee, T.; Knappik, A.; Sandford, E.; Tewari, M.; Choi, S. W.; Strong, W. B.; Thrush, E. P.; Oh, K. J.; Liu, N.; Walter, N. G.; Johnson-Buck, A. Direct kinetic fingerprinting and digital counting of single protein molecules. *Proc. Natl. Acad. Sci. U.S.A.* **2020**, *117* (37), 22815−22822.

NOTE ADDED AFTER ISSUE PUBLICATION

Due to a production editor this paper was published in volume 22, issue 15, without all the authors' corrections made. The corrected version was reposted on September 21, 2022 with an Addition/Correction.

https://doi.org/10.1021/acs.nanolett.2c01757
Nano Lett. 2022, 22, 6235−6244